Self-splitting properties of a Hermite-Gaussian correlated Schell-model beam

Yahong Chen, Jiaxin Gu, Fei Wang, and Yangjian Cai[*]

*School of Physical Science and Technology and Collaborative Innovation Center of Suzhou Nano Science and Technology,
Soochow University, Suzhou 215006, China*

We introduce one kind of partially coherent beam with a nonconventional correlation function named the Hermite-Gaussian correlated Schell-model (HGCSM) beam. It is found that a HGCSM beam exhibits self-splitting properties on propagation in free space, i.e., the initial single beam spot evolves into two or four beam spots in the far field depending on the initial beam orders, which are closely related to the beam width and coherence widths of the HGCSM beam, and a focused HGCSM beam exhibits splitting and combining properties near the focal plane. Furthermore, we report experimental generation of a HGCSM beam and demonstrate splitting and combining properties of a focused HGCSM beam in experiment. The phenomenon of correlation-induced self-splitting will be useful for attacking multiple targets, trapping multiple particles, and guiding atoms.

I. INTRODUCTION

It is well known that the propagation properties of a laser beam are closely determined by its amplitude, polarization, and phase. A laser beam with prescribed amplitude can display extraordinary properties; e.g., a Bessel beam exhibits the properties of nondiffraction and self-healing [1–3], and an Airy beam exhibits the properties of self-acceleration, nondiffraction, and self-healing [4–7]. A laser beam with spatially nonuniform state of polarization exhibits interesting and useful tightly focusing properties. For example, when a radially polarized beam is focused by a high-numerical-aperture (NA) lens, a strong longitudinal electric field appears and the tightly focused beam spot is much smaller than that of a linearly polarized beam [8–10], and when an azimuthally polarized beam is focused by a high-NA lens, a strong magnetic field on the optical axis is generated while the electric field is purely transverse and displays subwavelength dark channel [11,12]. A laser beam with vortex phase can carry an orbital angular momentum [13] which is useful in free-space information transfer and communications [14], quantum information processing and quantum cryptography [15], and optical manipulation [16].

High coherence is an important property of a laser beam, while a laser beam with coherence (i.e., partially coherent beam) is preferred in some applications, such as inertial confinement fusion [17], optical imaging [18–20], atom cooling [21], atomic recoil lasing [22], free-space optical communications [23], particle trapping [24,25], optical scattering [26,27], and second-harmonic generation [28,29]. When the coherence of a beam is reduced, some interesting phenomena can appear; e.g., the degree of polarization and the state of polarization of a vector partially coherent beam varies on propagation [30,31], spectral shift appears in a polychromatic partially coherent beam on propagation [32,33], and a unique twist phase can exist in a partially coherent beam and such beam possesses orbital angular momentum [34,35].

The conventional correlation function of a partially coherent beam is a Gaussian correlated Schell-model function,

which has been studied in detail both theoretically and experimentally in the past decades [30,36–38]. Since Gori *et al.* discussed the sufficient condition for devising a genuine correlation function of a partially coherent beam [39,40], more and more attention is being paid to partially coherent beams with nonconventional correlation functions [41–51]. Partially coherent beams with nonconventional correlation functions have displayed many extraordinary properties [41], such as self-focusing and lateral shift of the intensity maximum [42], far-field prescribed beam profile formation [43–47], reduction of scintillation in turbulence [48,49], far-field radially polarization formation [50], and controllable optical cage formation near the focal plane [51].

Conventionally one usually uses anisotropic optical components or structures such as a beam splitter, photonic crystal [52], anisotropic metamaterial slab [53], plane-parallel absorptive slab [54], and metallic nano-optic lens [55] and gratings [56] to split one beam into two or more beams, which are useful in many applications, such as ghost imaging [18], ghost interference [57], particle trapping [58], and atom guidance [59]. In this paper, we introduce one kind of partially coherent beam with nonconventional correlation function named Hermite-Gaussian correlated Schell-model (HGCSM) beam and report experimental generation of the proposed HGCSM beam. Both theoretical and experimental results show that the proposed HGCSM beam exhibits self-splitting properties, which will be useful for attacking multiple targets, trapping multiple particles, and guiding atoms.

II. HERMITE-GAUSSIAN CORRELATED SCHELL-MODEL BEAM AND ITS PROPAGATION FACTOR

In the space-time domain, the statistical properties of a scalar partially coherent beam are characterized by the mutual coherence function (MCF), which is defined as a two-point correlation function [36]:

$$J_0(\mathbf{r}_1,\mathbf{r}_2) = \langle E^*(\mathbf{r}_1)E(\mathbf{r}_2)\rangle, \qquad (1)$$

where E denotes the field fluctuating in a direction perpendicular to the z axis, and the angular brackets denote an ensemble average. To be a mathematically genuine correlation function,

---

[*]Corresponding author: yangjiancai@suda.edu.cn

the MCF must correspond to a non-negative definite kernel, which is fulfilled if the MCF function can be written in the form [39]

$$J_0(\mathbf{r}_1, \mathbf{r}_2) = \int I(\mathbf{v}) H^*(\mathbf{r}_1, \mathbf{v}) H(\mathbf{r}_2, \mathbf{v}) d^2\mathbf{v}, \qquad (2)$$

where H is an arbitrary kernel and I is a non-negative function.

Equation (2) can be expressed in the following alternative form [41,46]:

$$J_0(\mathbf{r}_1, \mathbf{r}_2) = \iint J_i(\mathbf{v}_1, \mathbf{v}_2) H^*(\mathbf{r}_1, \mathbf{v}_1) H(\mathbf{r}_2, \mathbf{v}_2) d^2\mathbf{v}_1 d^2\mathbf{v}_2, \qquad (3)$$

where

$$J_i(\mathbf{v}_1, \mathbf{v}_2) = \sqrt{I(\mathbf{v}_1)I(\mathbf{v}_2)}\delta(\mathbf{v}_1 - \mathbf{v}_2). \qquad (4)$$

Here δ denotes the Dirac delta function. Thus a partially coherent beam can be generated from an incoherent source with MCF J_i through propagation, and the MCF of the generated beam is modulated by H and I. Here H denotes the response function of the optical path and I denotes the intensity of the incoherent source.

If we set H and I as follows,

$$H(\mathbf{r}, \mathbf{v}) = -\frac{i}{\lambda f} T(\mathbf{r}) \exp\left[\frac{i\pi}{\lambda f}(\mathbf{v}^2 - 2\mathbf{r} \cdot \mathbf{v})\right], \qquad (5)$$

$$I(\mathbf{v}) = \left(\frac{v_x^2}{\omega_{0x}^2}\right)^m \left(\frac{v_y^2}{\omega_{0y}^2}\right)^n \exp\left[-\frac{2v_x^2}{\omega_{0x}^2} - \frac{2v_y^2}{\omega_{0y}^2}\right], \qquad (6)$$

$$T(\mathbf{r}) = \exp\left(-\frac{\mathbf{r}^2}{4\sigma_0^2}\right), \qquad (7)$$

where H represents the response function of the optical path which consists of free-space distance f, a thin lens with focal length f, and a Gaussian amplitude filter with transmission function T; I denotes the intensity of the incoherent source with ω_{0x} and ω_{0y} being the beam widths along the x and y directions, respectively, m and n being the beam orders, then substituting Eqs. (5)–(7) into Eqs. (3) and (4), we obtain the following expression for the MCF of the generated partially coherent beam:

$$J_0(\mathbf{r}_1, \mathbf{r}_2) = G_0 \exp\left[-\frac{\mathbf{r}_1^2 + \mathbf{r}_2^2}{4\sigma_0^2}\right]\gamma(\mathbf{r}_2 - \mathbf{r}_1), \qquad (8)$$

where G_0 is a constant, σ_0 denotes the beam width of the generated beam, and $\gamma(\mathbf{r}_2 - \mathbf{r}_1)$ represents the degree of coherence (DOC) of the generated beam and is given by

$$\gamma(\mathbf{r}_2 - \mathbf{r}_1) = \frac{H_{2m}[(x_2 - x_1)/\sqrt{2}\delta_{0x}]}{H_{2m}(0)} \exp\left[-\frac{(x_2 - x_1)^2}{2\delta_{0x}^2}\right]$$

$$\times \frac{H_{2n}[(y_2 - y_1)/\sqrt{2}\delta_{0y}]}{H_{2n}(0)} \exp\left[-\frac{(y_2 - y_1)^2}{2\delta_{0y}^2}\right], \qquad (9)$$

with $\delta_{0x} = \lambda f/\pi\omega_{0x}$ and $\delta_{0y} = \lambda f/\pi\omega_{0y}$ being the transverse coherence width along the x and y directions, respectively. Here H_m denotes the Hermite polynomial of order m. We call the partially coherent beam whose MCF is given by
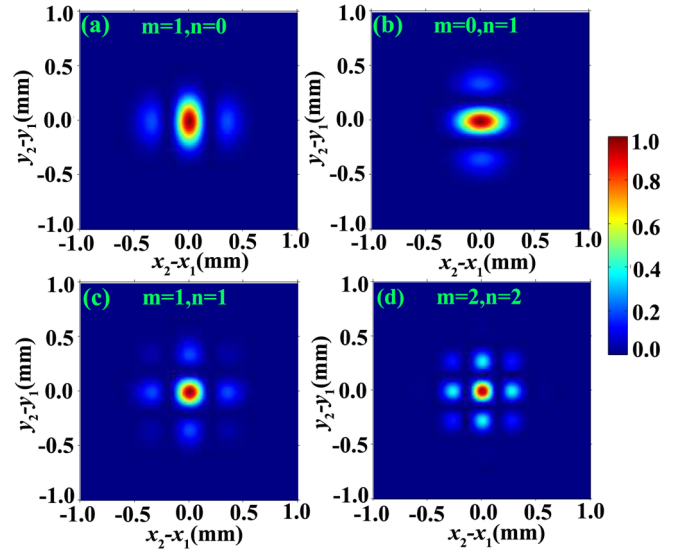
FIG. 1. (Color online) Density plot of the square of the modulus of the DOC of the HGCSM beam for different values of the beam orders m and n with $\delta_{0x} = \delta_{0y} = 0.2$ mm.

Eqs. (8) and (9) as a Hermite-Gaussian correlated Schell-model (HGCSM) beam. Under the condition of $m = n = 0$, the HGCSM beam reduces to the elliptical Gaussian correlated Schell-model beam [46]. Under the condition of $m = n = 0$ and $\delta_{0x} = \delta_{0y}$, the HGCSM beam reduces to the conventional Gaussian correlated Schell-model beam (also named Gaussian Schell-model beam) [36].

Figure 1 shows the density plot of the square of the modulus of the DOC of the proposed HGCSM beam for different values of the beam orders m and n with $\delta_{0x} = \delta_{0y} = 0.2$ mm. One finds that the DOC of the HGCSM beam has a non-Gaussian distribution as expected, and it exhibits array distribution with rectangular symmetry, and the number of the beamlets increases as the values of the beam order m and n increases. Due to the nonconventional correlation function (i.e., non-Gaussian distribution of the DOC), the HGCSM beam exhibits extraordinary propagation properties such as self-splitting as shown later, although it has the same intensity distribution with the conventional Gaussian correlated Schell-model beam in the source plane.

The propagation factor (also named M^2 factor) is an important property of a beam being regarded as a beam quality factor in many practical applications. Siegman first introduced the definition of the propagation factor of a coherent beam [60], and Gori et al. introduced the definition of the propagation factor of a partially coherent beam [61,62]. According to [61,62], the propagation factors of a HGCSM beam along the x and y directions are defined as

$$M_x^2 = 4\pi\sigma_{x0}\sigma_{x\infty}, \quad M_y^2 = 4\pi\sigma_{y0}\sigma_{y\infty}, \qquad (10)$$

where $\sigma_{\alpha 0}$ and $\sigma_{\alpha\infty}$ ($\alpha = x, y$) are the square roots of the variances of the transverse intensity profiles at the source plane and in the far field along the α direction, respectively, and can

be expressed as

$$\sigma_{x0}^2 = \frac{1}{\overline{I}} \int_{-\infty}^{\infty} \int_{-\infty}^{\infty} x^2 J_0(x,y,x,y) dx dy, \qquad (11)$$

$$\sigma_{y0}^2 = \frac{1}{\overline{I}} \int_{-\infty}^{\infty} \int_{-\infty}^{\infty} y^2 J_0(x,y,x,y) dx dy, \qquad (12)$$

$$\sigma_{x\infty}^2 = \frac{1}{4\pi^2 \overline{I}} \int_{-\infty}^{\infty} \int_{-\infty}^{\infty} \left[\frac{\partial J_0(x_1,y_1,x_2,y_2)}{\partial x_1 \partial x_2} \Big|_{\substack{x_1=x_2=x \\ y_1=y_2=y}} \right] dx dy, \qquad (13)$$

$$\sigma_{y\infty}^2 = \frac{1}{4\pi^2 \overline{I}} \int_{-\infty}^{\infty} \int_{-\infty}^{\infty} \left[\frac{\partial J_0(x_1,y_1,x_2,y_2)}{\partial y_1 \partial y_2} \Big|_{\substack{x_1=x_2=x \\ y_1=y_2=y}} \right] dx dy. \qquad (14)$$

Here $\overline{I}$ denotes the total power carried by the laser beam given by

$$\overline{I} = \int_{-\infty}^{\infty} \int_{-\infty}^{\infty} J_0(x,y,x,y) \, dx dy. \qquad (15)$$

Substituting Eqs. (8) and (9) into Eqs. (10)–(15), we obtain (after some operation) the following expressions for the propagation factors of HGCSM beam:

$$M_x^2 = \sqrt{4 \frac{\sigma_0^2}{\delta_{0x}^2} \left[1 - \frac{4m(2m-1)H_{2m-2}(0)}{H_{2m}(0)} \right] + 1}, \qquad (16)$$

$$M_y^2 = \sqrt{4 \frac{\sigma_0^2}{\delta_{0y}^2} \left[1 - \frac{4n(2n-1)H_{2n-2}(0)}{H_{2n}(0)} \right] + 1}. \qquad (17)$$

Under the condition of $m = n = 0$ and $\delta_{0x} = \delta_{0y}$, Eq. (16) or (17) reduces to the expression for the propagation factor of the conventional Gaussian correlated Schell-model beam [62]. It is clear from Eqs. (16) and (17) that M_x^2 depends on σ_0, δ_{0x}, m and M_y^2 depends on σ_0, δ_{0y}, n. Figure 2 shows the propagation factor M_x^2 of a HGCSM beam versus the beam order m for different values of the initial coherence width δ_{0x} with $\sigma_0 = 1$ mm. One sees that M_x^2 increases as the beam order m increases or as the coherence width δ_{0x} decreases. When $\delta_{0x} = \infty$, M_x^2 is equal to 1 which represents the propagation factor of a coherent Gaussian beam.
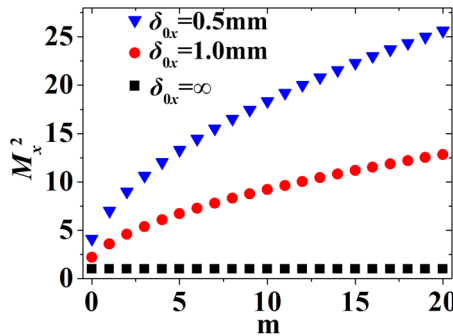
FIG. 2. (Color online) Propagation factor M_x^2 of a HGCSM beam versus the beam order m for different values of the initial coherence width δ_{0x}.

III. PARAXIAL PROPAGATION OF A HERMITE-GAUSSIAN CORRELATED SCHELL-MODEL BEAM

In this section, we derive the paraxial propagation formula for the MCF of a HGCSM beam passing through a stigmatic $ABCD$ optical system.

Paraxial propagation of the MCF of a partially coherent beam through a stigmatic $ABCD$ optical system can be treated by the following generalized Collins formula [63,64]:

$$J(\boldsymbol{\rho}_1, \boldsymbol{\rho}_2) = \frac{1}{(\lambda B)^2} \exp\left[-\frac{ikD}{2B} (\boldsymbol{\rho}_1^2 - \boldsymbol{\rho}_2^2) \right]$$
$$\times \int_{-\infty}^{\infty} \int_{-\infty}^{\infty} J_0(\mathbf{r}_1, \mathbf{r}_2) \exp\left[-\frac{ikA}{2B} (\mathbf{r}_1^2 - \mathbf{r}_2^2) \right]$$
$$\times \exp\left[\frac{ik}{B} (\mathbf{r}_1 \cdot \boldsymbol{\rho}_1 - \mathbf{r}_2 \cdot \boldsymbol{\rho}_2) \right] d^2\mathbf{r}_1 d^2\mathbf{r}_2, \qquad (18)$$

where $\boldsymbol{\rho}_1 \equiv (\rho_{1x}, \rho_{1y})$ and $\boldsymbol{\rho}_2 \equiv (\rho_{2x}, \rho_{2y})$ are the two arbitrary transverse position vectors in the output plane; A, B, C, D are the elements of the transfer matrix for the stigmatic optical system; $k = 2\pi/\lambda$ is the wave number; and λ is the wavelength.

For the convenience of integration, we introduce the following "sum" and "difference" coordinates:

$$x_s = (x_1 + x_2)/2, \quad \Delta x = x_1 - x_2, \qquad (19)$$

$$y_s = (y_1 + y_2)/2, \quad \Delta y = y_1 - y_2. \qquad (20)$$

Substituting Eqs. (8), (9), (19), and (20) into (18), we obtain

$$J(\boldsymbol{\rho}_1, \boldsymbol{\rho}_2, z)$$
$$= \frac{G_0}{(\lambda B)^2} \exp\left[-\frac{ikD}{2B} (\boldsymbol{\rho}_1^2 - \boldsymbol{\rho}_2^2) \right]$$
$$\times \int_{-\infty}^{\infty} \int_{-\infty}^{\infty} \int_{-\infty}^{\infty} \int_{-\infty}^{\infty} P^*\left(x_s + \frac{\Delta x}{2} \right) P\left(x_s - \frac{\Delta x}{2} \right) g_x(\Delta x)$$
$$\times \exp\left\{ \frac{ik}{B} \left[\left(x_s + \frac{\Delta x}{2} \right) \rho_{1x} - \left(x_s - \frac{\Delta x}{2} \right) \rho_{2x} \right] \right\}$$
$$\times P^*\left(y_s + \frac{\Delta y}{2} \right) P\left(y_s - \frac{\Delta y}{2} \right) g_y(\Delta y)$$
$$\times \exp\left\{ \frac{ik}{B} \left[\left(y_s + \frac{\Delta y}{2} \right) \rho_{1y} - \left(y_s - \frac{\Delta y}{2} \right) \rho_{2y} \right] \right\}$$
$$\times d\Delta x dx_s d\Delta y dy_s, \qquad (21)$$

where

$$P^*(S) = \exp\left[-\left(\frac{1}{4\sigma_0^2} + \frac{ikA}{2B} \right) S^2 \right],$$
$$S = (x_s + \Delta x/2, y_s + \Delta y/2), \qquad (22)$$

$$P(D) = \exp\left[-\left(\frac{1}{4\sigma_0^2} - \frac{ikA}{2B}\right)D^2\right],$$

$$D = (x_s - \Delta x/2, y_s - \Delta y/2), \tag{23}$$

$$g_x(\Delta x) = \frac{H_{2m}(\Delta x/\sqrt{2}\delta_{0x})}{H_{2m}(0)} \exp\left(-\frac{\Delta x^2}{2\delta_{0x}^2}\right), \tag{24}$$

$$g_y(\Delta y) = \frac{H_{2n}(\Delta y/\sqrt{2}\delta_{0y})}{H_{2n}(0)} \exp\left(-\frac{\Delta y^2}{2\delta_{0y}^2}\right). \tag{25}$$

$P^*(S)$ and $P(D)$ can be expressed in the terms of their Fourier transforms $\widetilde{P}^*(U_1/\lambda B)$ and $\widetilde{P}(U_2/\lambda B)$ as follows:

$$P^*(S) = \frac{1}{\lambda B}\int_{-\infty}^{\infty} \widetilde{P}^*\left(\frac{U_1}{\lambda B}\right)\exp\left(\frac{ik}{B}SU_1\right)dU_1,$$

$$U_1 = (u_{1x}, u_{1y}), \tag{26}$$

$$P(D) = \frac{1}{\lambda B}\int_{-\infty}^{\infty} \widetilde{P}\left(\frac{U_2}{\lambda B}\right)\exp\left(-\frac{ik}{B}DU_2\right)dU_2,$$

$$U_2 = (u_{2x}, u_{2y}). \tag{27}$$

Substituting Eqs. (26) and (27) into (21), after some operation, Eq. (21) can be expressed as

$$J(\boldsymbol{\rho}_1, \boldsymbol{\rho}_2) = \frac{G_0}{(\lambda B)^4}\exp\left[-\frac{ikD}{2B}(\boldsymbol{\rho}_1^2 - \boldsymbol{\rho}_2^2)\right]$$

$$\times \int_{-\infty}^{\infty}\int_{-\infty}^{\infty} \widetilde{P}^*\left(\frac{u_{1x}}{\lambda B}\right)\widetilde{P}\left[\frac{(u_{1x} + \rho_{1x} - \rho_{2x})}{\lambda B}\right]$$

$$\times \widetilde{g}_x\left(-\frac{\rho_{1x} + u_{1x}}{\lambda B}\right)$$

$$\times \widetilde{P}^*\left(\frac{u_{1y}}{\lambda B}\right)\widetilde{P}\left[\frac{(u_{1y} + \rho_{1y} - \rho_{2y})}{\lambda B}\right]\widetilde{g}_y\left(-\frac{\rho_{1y} + u_{1y}}{\lambda B}\right)$$

$$\times du_{1x}du_{1y}, \tag{28}$$

where $\widetilde{g}_x$ or $\widetilde{g}_y$ represents the Fourier transform of g_x or g_y, and

$$\widetilde{P}^*\left(\frac{u_{1x}}{\lambda B}\right) = \sqrt{\pi}\sigma^*(B)\exp\left[-\frac{\pi^2\sigma^{*2}(B)}{(\lambda B)^2}u_{1x}^2\right], \tag{29}$$

$$\widetilde{P}^*\left(\frac{u_{1y}}{\lambda B}\right) = \sqrt{\pi}\sigma^*(B)\exp\left[-\frac{\pi^2\sigma^{*2}(B)}{(\lambda B)^2}u_{1y}^2\right], \tag{30}$$

$$\widetilde{P}\left[\frac{(u_{1x} + \rho_{1x} - \rho_{2x})}{\lambda B}\right]$$

$$= \sqrt{\pi}\sigma(B)\exp\left[-\frac{\pi^2\sigma^2(B)}{(\lambda B)^2}(u_{1x} + \rho_{1x} - \rho_{2x})^2\right], \tag{31}$$

$$\widetilde{P}\left[\frac{(u_{1y} + \rho_{1y} - \rho_{2y})}{\lambda B}\right]$$

$$= \sqrt{\pi}\sigma(B)\exp\left[-\frac{\pi^2\sigma^2(B)}{(\lambda B)^2}(u_{1y} + \rho_{1y} - \rho_{2y})^2\right], \tag{32}$$

$$\widetilde{g}_x\left(-\frac{\rho_{1x} + u_{1x}}{\lambda B}\right) = \frac{\sqrt{2\pi}2^{2m}\delta_{0x}}{H_{2m}(0)}\left[-\frac{2\delta_{0x}^2\pi^2}{(\lambda B)^2}(\rho_{1x} + u_{1x})^2\right]^m$$

$$\times \exp\left[-\frac{2\delta_{0x}^2\pi^2}{(\lambda B)^2}(\rho_{1x} + u_{1x})^2\right], \tag{33}$$

$$\widetilde{g}_y\left(-\frac{\rho_{1y} + u_{1y}}{\lambda B}\right) = \frac{\sqrt{2\pi}2^{2n}\delta_{0y}}{H_{2n}(0)}\left[-\frac{2\delta_{0x}^2\pi^2}{(\lambda B)^2}(\rho_{1y} + u_{1y})^2\right]^n$$

$$\times \exp\left[-\frac{2\delta_{0y}^2\pi^2}{(\lambda B)^2}(\rho_{1y} + u_{1y})^2\right], \tag{34}$$

with $\sigma(B) = (1/4\sigma_0^2 - ikA/2B)^{-1/2}$.

After tedious integration over u_{1x} and u_{1y} in Eq. (28), we obtain the following expression for the MCF of the HGCSM beam in the output plane:

$$J(\boldsymbol{\rho}_1, \boldsymbol{\rho}_2, z) = \frac{G_0}{H_{2m}(0)H_{2n}(0)}\left(\frac{\pi}{\lambda B}\right)^2\exp\left[-\frac{ikD}{2B}(\boldsymbol{\rho}_1^2 - \boldsymbol{\rho}_2^2)\right]2^{m+n+1}\sigma^{*2}(B)\sigma^2(B)\delta_{0x}^{2m+1}\delta_{0y}^{2n+1}\delta_x^{-(2m+1)}(B)\delta_y^{-(2n+1)}(B)$$

$$\times \exp\left\{-\left(\frac{\pi}{\lambda B}\right)^2[\sigma^{*2}(B)\rho_{1x}^2 + \sigma^2(B)\rho_{2x}^2]\right\}\exp\left\{-\left(\frac{\pi}{\lambda B}\right)^2[\sigma^{*2}(B)\rho_{1y}^2 + \sigma^2(B)\rho_{2y}^2]\right\}$$

$$\times \exp\left\{\left(\frac{\pi}{\lambda B}\right)^2\frac{[\sigma^{*2}(B)\rho_{1x} + \sigma^2(B)\rho_{2x}]^2}{\delta_x^2(B)}\right\}H_{2m}\left\{i\left(\frac{\pi}{\lambda B}\right)\frac{[\sigma^{*2}(B)\rho_{1x} + \sigma^2(B)\rho_{2x}]}{\delta_x(B)}\right\}$$

$$\times \exp\left\{\left(\frac{\pi}{\lambda B}\right)^2\frac{[\sigma^{*2}(B)\rho_{1y} + \sigma^2(B)\rho_{2y}]^2}{\delta_y^2(B)}\right\}H_{2n}\left\{i\left(\frac{\pi}{\lambda B}\right)\frac{[\sigma^{*2}(B)\rho_{1y} + \sigma^2(B)\rho_{2y}]}{\delta_y(B)}\right\}, \tag{35}$$

with $\delta_x(B) = \sqrt{\sigma^{*2}(B) + \sigma^2(B) + 2\delta_{0x}^2}$ and $\delta_y(B) = \sqrt{\sigma^{*2}(B) + \sigma^2(B) + 2\delta_{0y}^2}$.

The average intensity of the HGCSM beam in the output plane is obtained as

$$I(\boldsymbol{\rho}, z) = J(\boldsymbol{\rho}, \boldsymbol{\rho}, z). \tag{36}$$

Applying Eqs. (35) and (36), we can study the propagation properties of a HGCSM beam passing through a stigmatic $ABCD$ optical system numerically in a convenient way.
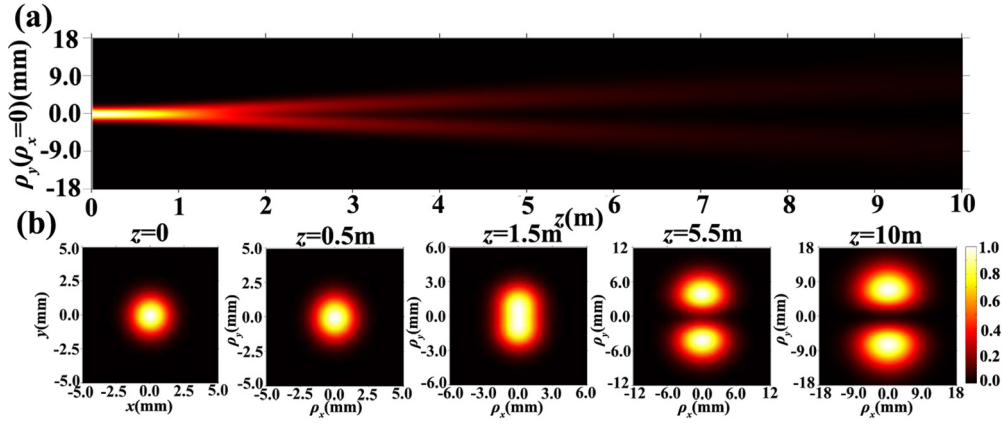
FIG. 3. (Color online) Normalized intensity distributions of a HGCSM beam with $m = 0$, $n = 1$, $\delta_{0x} = \delta_{0y} = 0.2$ mm (a) in the $\rho_y - z$ plane on propagation, and (b) in the $\rho_x - \rho_y$ plane at several propagation distances in free space.

IV. SELF-SPLITTING PROPERTIES OF A HERMITE-GAUSSIAN CORRELATED SCHELL-MODEL BEAM

In this section, we study the propagation properties of a HGCSM beam by applying the formulas derived in Sec. III. First we study the propagation properties of a HGCSM beam in free space. The transfer matrix for free space of distance z is expressed as

$$\begin{pmatrix} A & B \\ C & D \end{pmatrix} = \begin{pmatrix} 1 & z \\ 0 & 1 \end{pmatrix}. \tag{37}$$

Applying Eqs. (35)–(37), we calculate in Figs. 3–6 the normalized intensity distribution of a HGCSM beam on propagation in free space for different values of the beam orders m and n with $\delta_{0x} = \delta_{0y} = 0.2$ mm, $\sigma_0 = 1$ mm, and $\lambda = 632.8$ nm. One finds from Figs. 3–6 that the HGCSM beam exhibits self-splitting properties on propagation in free space; i.e., the initial one beam spot evolves into two or four beam spots in the far field depending on the initial beam orders, which are quite different from the propagation properties of the conventional Gaussian correlated Schell-model beam. The intensity distribution of the conventional Gaussian correlated Schell-model beam always has a Gaussian beam profile on propagation. For

the case of $m = 0$ and $n = 1$ or $m = 1$ and $n = 0$, the beam spot of the HGCSM beam is split into two beam spots in the far field. For the case of $m \geqslant 1$ and $n \geqslant 1$, the beam spot of the HGCSM beam is split into four beam spots in the far field, which is similar to the properties of a cosine Gaussian correlated Schell-model beam with rectangular symmetry in the far field [47]. Thus we can call the HGCSM beam as a self-splitting beam. The self-splitting properties of the HGCSM beam are induced by the nonconventional correlation function (i.e., non-Gaussian distribution of the DOC) and can be used to attack multiple targets with the initial one beam spot in free space.

The self-splitting properties of the HGCSM beam are closely related to the beam width σ_0 and coherence widths δ_{0x} and δ_{0y} of the Hermite-Gaussian correlated Schell-model (HGCSM) beam. Figure 7 shows the normalized intensity distribution of a HGCSM beam with $m = 1$, $n = 1$, and $\delta_{0x} = \delta_{0y} = 0.2$ mm on propagation in free space for different values of σ_0. Figure 8 shows the normalized intensity distribution of a HGCSM beam with $m = 1$, $n = 1$, $\sigma_0 = 1$ mm on propagation in free space for different values of δ_{0x} and δ_{0y}. One sees from Figs. 7 and 8 that the self-splitting properties of the HGCSM beam on propagation gradually disappear as the beam width decreases or the transverse coherence widths increase when the beam width is smaller than the
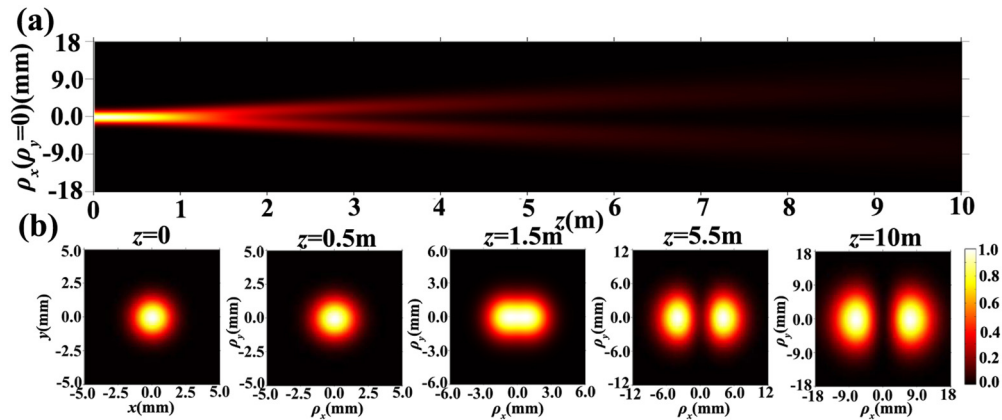
FIG. 4. (Color online) Normalized intensity distributions of a HGCSM beam with $m = 1$, $n = 0$, $\delta_{0x} = \delta_{0y} = 0.2$ mm (a) in the $\rho_x - z$ plane on propagation, and (b) in the $\rho_x - \rho_y$ plane at several propagation distances in free space.
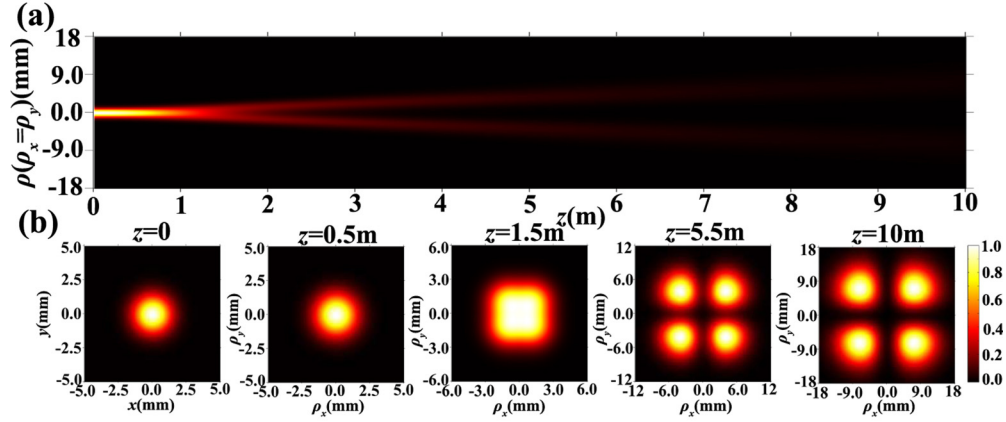
FIG. 5. (Color online) Normalized intensity distributions of a HGCSM beam with $m = 1$, $n = 1$, $\delta_{0x} = \delta_{0y} = 0.2$ mm (a) in the $\rho - z$ plane with $\rho_x = \rho_y$ on propagation, and (b) in the $\rho_x - \rho_y$ plane at several propagation distances in free space.
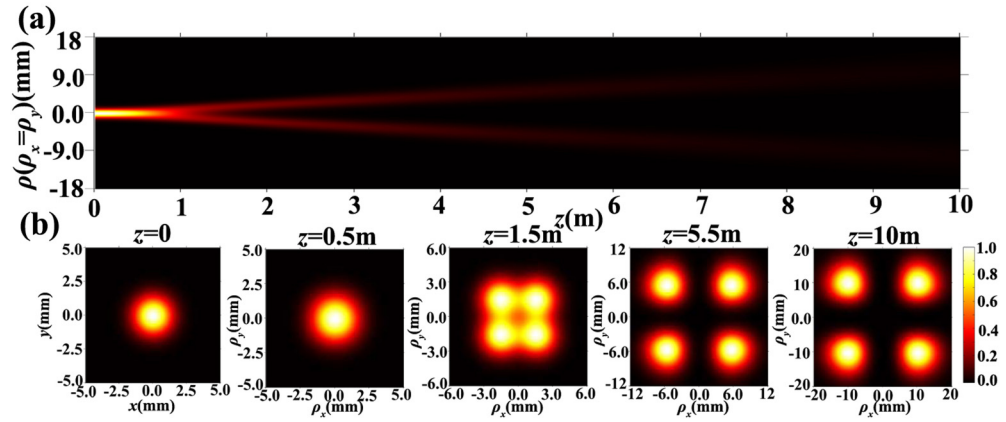
FIG. 6. (Color online) Normalized intensity distributions of a HGCSM beam with $m = 2$, $n = 2$, $\delta_{0x} = \delta_{0y} = 0.2$ mm (a) in the $\rho - z$ plane with $\rho_x = \rho_y$ on propagation, and (b) in the $\rho_x - \rho_y$ plane at several propagation distances in free space.
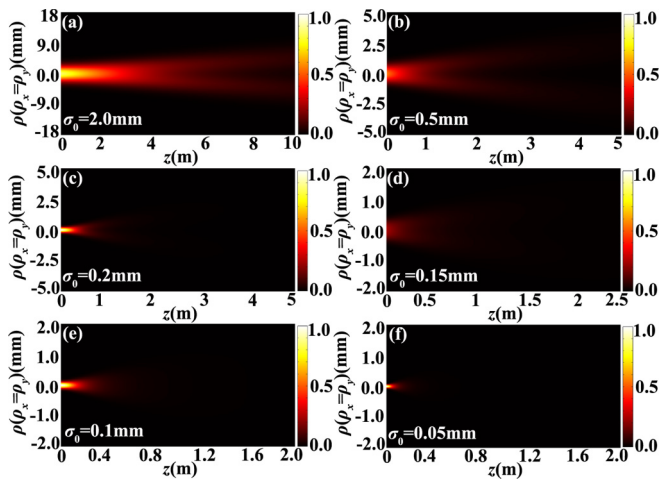
FIG. 7. (Color online) Normalized intensity distributions of a HGCSM beam with $m = 1$, $n = 1$, and $\delta_{0x} = \delta_{0y} = 0.2$ mm in the $\rho - z$ plane with $\rho_x = \rho_y$ on propagation in free space for different values of σ_0.
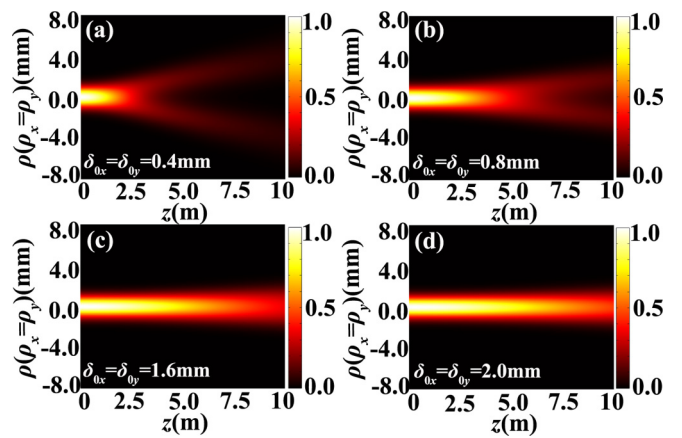
FIG. 8. (Color online) Normalized intensity distributions of a HGCSM beam with $m = 1$, $n = 1$, $\sigma_0 = 1$ mm in the $\rho - z$ plane with $\rho_x = \rho_y$ on propagation in free space for different values of δ_{0x} and δ_{0y}.
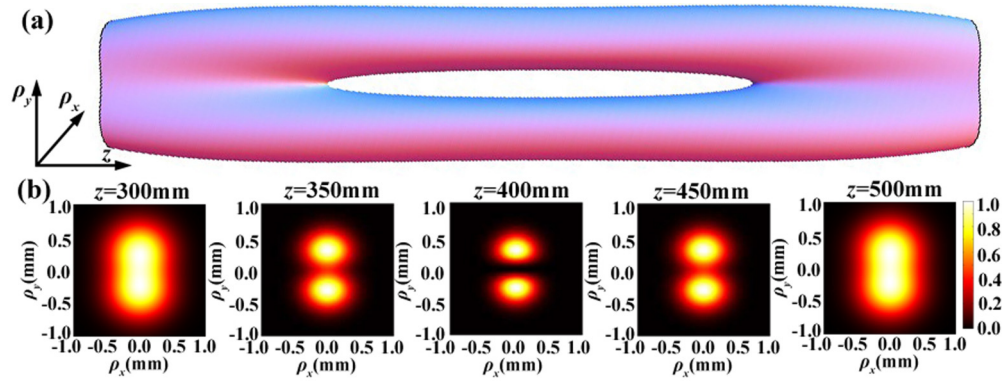
FIG. 9. (Color online) Normalized intensity distributions of a focused HGCSM beam with $m = 0$, $n = 1$, and $\delta_{0x} = \delta_{0y} = 0.2$ mm (a) in the $\rho_x - \rho_y - z$ plane on propagation, and (b) in the $\rho_x - \rho_y$ plane at several propagation distances in free space.

coherence widths. Thus it is necessary to choose suitable values of the beam width and the transverse coherence width to observe the self-splitting phenomenon on propagation. We should point out that our numerical results and conclusion are obtained under the condition of paraxial propagation (i.e., $\sigma_0 \gg \lambda$).

Now we study the focusing properties of a HGCSM beam. We assume that a HGCSM beam originating from the source plane ($z = 0$) is focused by a thin lens with focal length f. The distance between the source plane and the thin lens is f and the distance between the thin lens and the output plane is z. Then the transfer matrix between the source plane and the output plane is expressed as

$$\begin{pmatrix} A & B \\ C & D \end{pmatrix} = \begin{pmatrix} 1 & z \\ 0 & 1 \end{pmatrix} \begin{pmatrix} 1 & 0 \\ -1/f & 1 \end{pmatrix} \begin{pmatrix} 1 & f \\ 0 & 1 \end{pmatrix}$$
$$= \begin{pmatrix} 1 - z/f & f \\ -1/f & 0 \end{pmatrix}. \tag{38}$$

Applying Eqs. (35), (36), and (38), we calculate in Figs. 9 and 10 the normalized intensity distribution of a HGCSM beam after passing through a thin lens with focal length $f = 400$ mm on propagation for different values of the beam orders m and n with $\delta_{0x} = \delta_{0y} = 0.2$ mm. It is interesting to find that the beam spot of a focused HGCSM beam exhibits splitting properties before the focal plane ($z = 400$ mm),

while it exhibits combining properties after the focal plane. Before the focal plane, the initial one beam spot gradually becomes two or four beam spots, and the two or four beam spots gradually converge to one beam spot after the focal plane.

To learn about the influence of the focal length f of the thin lens on the splitting and combining properties of a focused HGCSM beam, we calculate in Fig. 11 the normalized intensity distribution of a focused HGCSM beam with $m = 1$, $n = 1$, and $\delta_{0x} = \delta_{0y} = 0.2$ mm on propagation in free space for different values of the focal length f of the thin lens. One finds that the splitting and combining properties of a focused HGCSM beam always exist for different values of the focal length f of the thin lens, while the focal length f affects the size of the beam spot in the focal plane. In our case, there is no aperture confinement on the thin lens; thus the numerical aperture (NA) of the thin lens is assumed to be zero. With the increase of the NA of the thin lens, the paraxial propagation formula in this paper gradually becomes invalid, and one should use the Richards-Wolf vectorial diffraction integral to treat the tight focusing of a HGCSM beam. Thus, our numerical results and conclusion are valid in the paraxial region.

The splitting and combining properties of the focused HGCSM beam are quite interesting and may be useful, for in some applications, e.g., it can be used to trap multiple
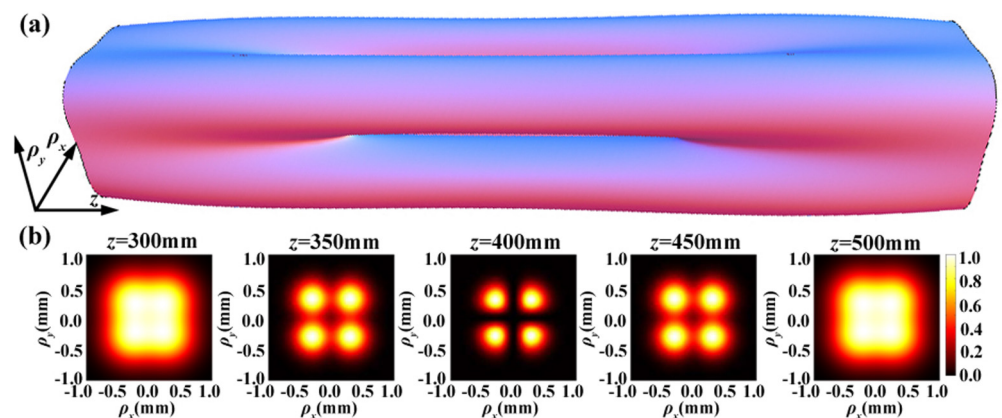
FIG. 10. (Color online) Normalized intensity distributions of a focused HGCSM beam with $m = 1$, $n = 1$, and $\delta_{0x} = \delta_{0y} = 0.2$ mm (a) in the $\rho_x - \rho_y - z$ plane on propagation, and (b) in the $\rho_x - \rho_y$ plane at several propagation distances.
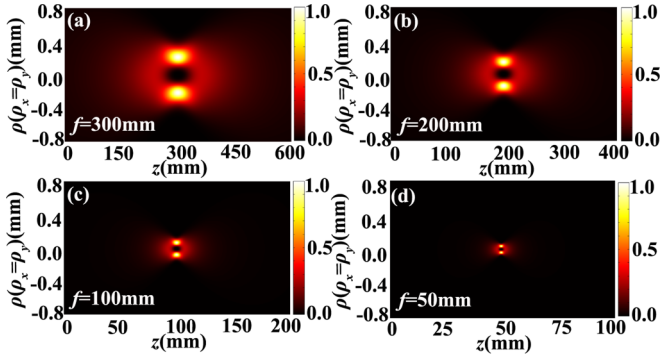
FIG. 11. (Color online) Normalized intensity distribution of a focused HGCSM beam with $m = 1$, $n = 1$, $\delta_{0x} = \delta_{0y} = 0.2$ mm in the $\rho - z$ plane with $\rho_x = \rho_y$ on propagation in free space for different values of the focal length f of the thin lens.

particles simultaneously in the focal plane, and it can be used to guide atoms along two or four channels near the focal plane. Furthermore, the HGCSM beam also can be used to bypass the small obstacle located in the beam center near the focal plane. Anyway, due to its extraordinary propagation properties, the HGCSM beam will be useful for trapping particles and guiding atoms.

V. EXPERIMENTAL DEMONSTRATION OF THE SPLITTING AND COMBINING PROPERTIES OF A HERMITE-GAUSSIAN CORRELATED SCHELL-MODEL BEAM

In this section, we carry out experimental generation of a HGCSM beam and carry out experimental demonstration of the splitting and combining properties of a focused HGCSM beam.

The experimental setup for generating a HGCSM beam, measuring the square of the modulus of its degree of coherence and its focused intensity is shown in Fig. 12. A laser beam ($\lambda = 632.8$ nm) emitted from a He-Ne laser passes through a beam expander, and illuminates a spatial light modulator (SLM, Holoeye LC2002); then diffraction patterns appear. Here the SLM acts as a phase grating designed by the method
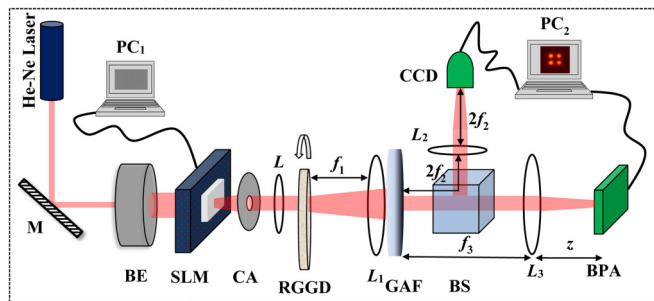
FIG. 12. (Color online) Experimental setup for generating a HGCSM beam, measuring the square of the modulus of its degree of coherence and its focused intensity. RM, reflecting mirror; BE, beam expander; SLM, spatial light modulator; CA, circular aperture; RGGD, rotating ground disk; L, L_1, L_2, L_3, thin lenses; GAF, Gaussian amplitude filter; BS, beam splitter; CCD, charge-coupled device; BPA, beam profile analyzer; PC_1, PC_2, personal computers.
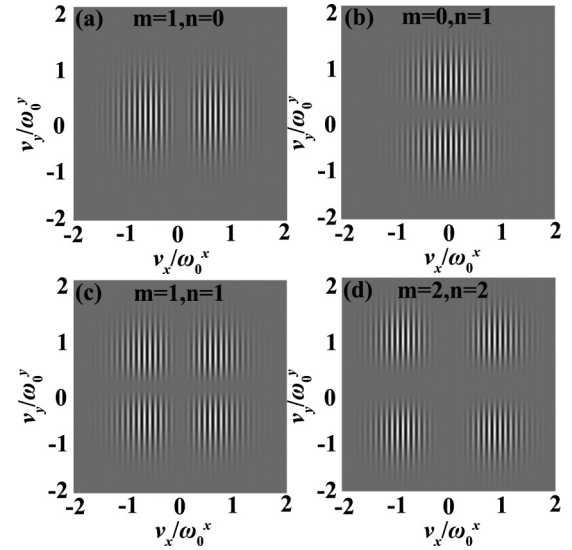
FIG. 13. Phase grating for the beam whose intensity is given by Eq. (6) with different values of the beam orders m and n. (a) $m = 1$, $n = 0$; (b) $m = 0$, $n = 1$; (c) $m = 1$, $n = 1$; (d) $m = 2$, $n = 2$.

of computer-generated holograms. The grating pattern of the holograms loaded on the SLM is calculated by the interference of a plane wave and a beam whose intensity is given by Eq. (6), and the phase grating for the beam whose intensity is given by Eq. (6) with different values of the beam orders m and n, are shown in Fig. 13. The first-order diffraction pattern is regarded as the beam whose intensity is given by Eq. (6) and selected out by a circular aperture (CA). The transmitted beam from the CA first goes through a thin lens L and then illuminates a rotating ground glass (RGGD) producing an incoherent beam whose intensity is given by Eq. (6). The output beam from the RGGD can be regarded as an incoherent beam under the condition that the diameter of the beam spot on the RGGD is larger than the inhomogeneity scale of the RGGD [65], which is satisfied in our experiment. Here L is used to control the beam spot size on the RGGD. The output beam from the RGGD passes through free space of distance f_1, a thin lens with focal length f_1, and a Gaussian amplitude filter, then becomes a HGCSM beam.

The generated HGCSM beam from the GAF is split into two beams by a beam splitter (BS). The reflected beam from the BS passes through a thin lens L_2 with focal length f_2, and
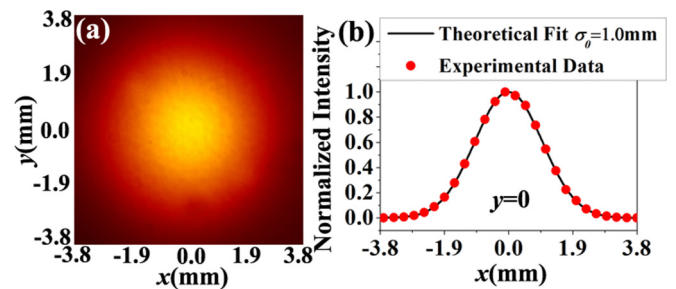
FIG. 14. (Color online) Experimental results of (a) the intensity distribution and (b) the corresponding cross line (dotted curve) of the generated HGCSM beam just behind the GAF. The solid curve denotes the theoretical fit of the experimental results with $\sigma_0 = 1$ mm.
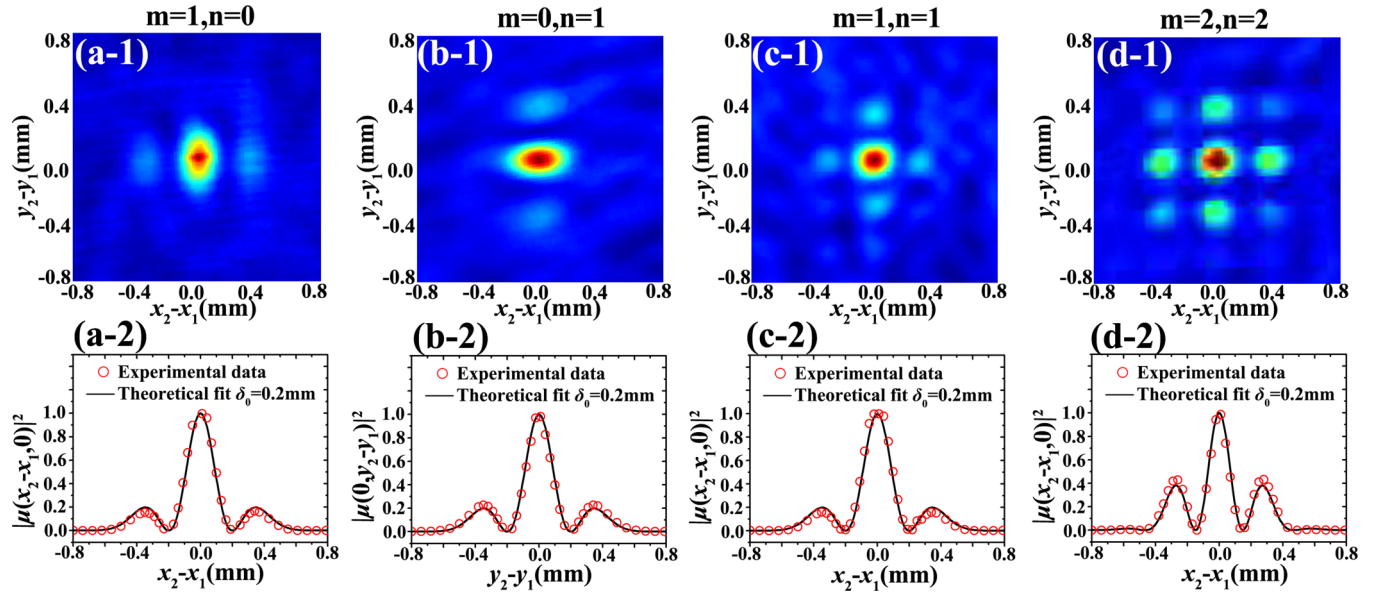
FIG. 15. (Color online) Experimental results of the square of the modulus of the DOC of the generated HGCSM beam for different values of the beam order m and n and the corresponding cross line (dotted curve). The solid line denotes the theoretical fit of the experimental results with $\delta_0 = 0.2$ mm.

goes towards a charge-coupled device (CCD), which is used to measure the square of the modulus of the DOC of the generated HGCSM beam. The detailed principle and measuring process can be found in [41,50].

The transmitted beam from the BS goes through a thin lens L_3 with focal length $f_3 = 400$ mm and arrives at a beam profile analyzer (BPA), which is used to measure the intensity distribution of the focused HGCSM beam on propagation. The
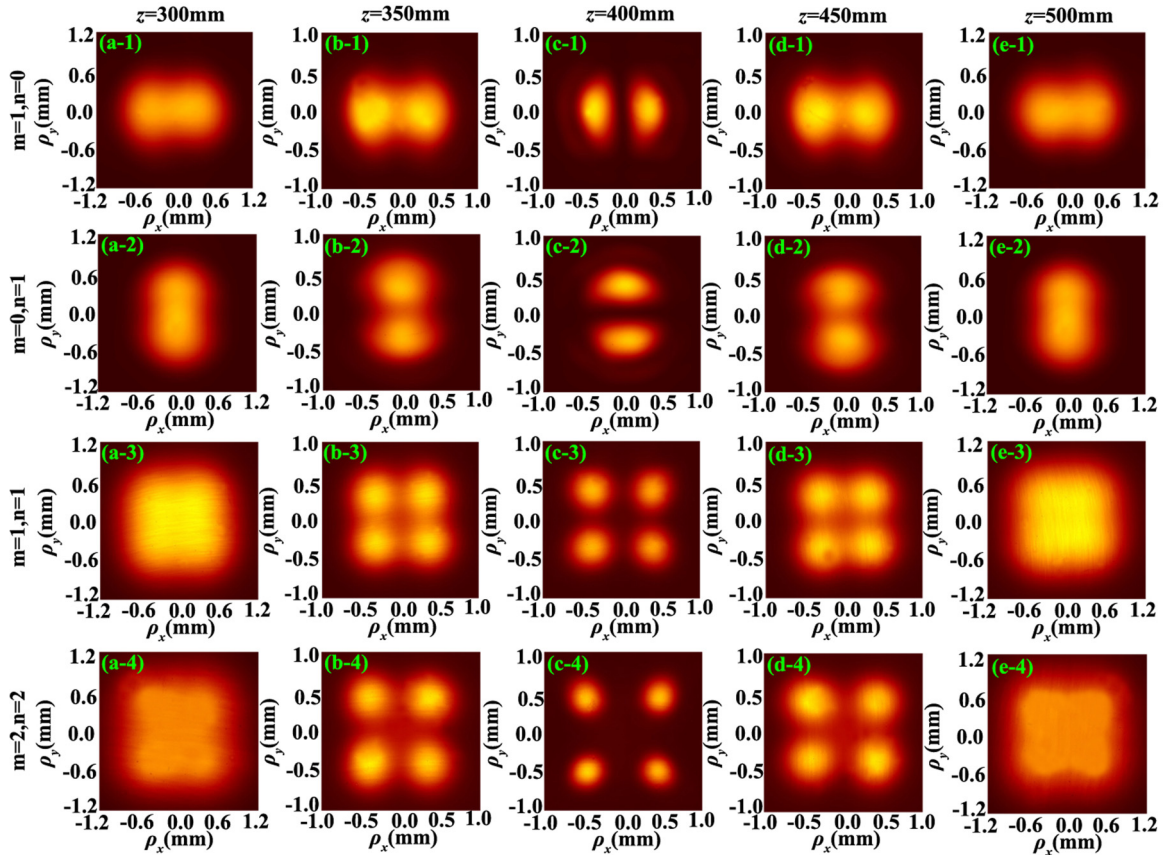
FIG. 16. (Color online) Experimental results of the intensity distribution of a focused HGCSM beam for different values of m and n with $\sigma_0 = 1$ mm and $\delta_0 = 0.2$ mm at several propagation distances.

distance from the GAF to L_3 is equal to f_3 and the distance from L_3 to the BPA is equal to z; thus the transfer matrix between the GAF and the BPA is given by Eq. (38) just by replacing f with f_3.

Figure 14 shows our experimental results of the intensity distribution and the corresponding line (dotted curve) of the generated HGCSM beam just behind the GAF. As expected, the intensity distribution of the generated HGCSM beam has a Gaussian beam profile at the source plane (just behind the GAF) and its beam width is determined by the transmission function of the GAF. Through theoretical fit (solid curve) of the experimental results, we obtain $\sigma_0 = 1$ mm. Figure 15 shows our experimental results of the square of the modulus of the DOC of the generated HGCSM beam for different values of the beam order m and n and the corresponding cross line (dotted curve). As expected, the DOC of the generated HGCSM beam at the source plane has a non-Gaussian distribution, and exhibits array distribution with rectangular symmetry, and the number of the beamlets increases as the values of the beam order m and n increases. Through theoretical fit of the experimental results, we obtain $\delta_0 = 0.2$ mm.

Figure 16 shows our experimental results of the intensity distribution of a focused HGCSM beam for different values of m and n with $\sigma_0 = 1$ mm and $\delta_0 = 0.2$ mm at several propagation distances. As expected, the focused HGCSM beam exhibits splitting and combining properties near the focal plane. In the focal plane, its beam spot exhibits two-beamlets array distribution for the case of $m = 0$ and $n = 1$ or $m = 1$ and $n = 0$, and its beam spot exhibits four-beamlets array distribution for the case of $m \geqslant 1$ and $n \geqslant 1$. Our experimental results are consistent with the theoretical predictions.

VI. CONCLUSION

We have introduced one kind of partially coherent beam with nonconventional correlation function, named the HGCSM beam, and studied its paraxial propagation properties. We have found that the HGCSM beam exhibits quite interesting propagation properties; e.g., a HGCSM beam exhibits self-splitting properties on propagation in free space, and a focused HGCSM beam exhibits splitting and combining properties near the focal plane. We have reported experimental generation of a HGCSM beam and demonstrated the splitting and combining properties of a focused HGCSM beam in experiment. The self-splitting properties of a HGCSM beam on propagation in free space can be used to attack multiple targets if the power of the beam is enough large. The splitting and combining properties of a focused HGCSM beam can be used for trapping particles and guiding atoms.

ACKNOWLEDGMENTS

[1] J. Durnin, J. J. Miceli, Jr. and J. H. Eberly, Diffraction-free beams, Phys. Rev. Lett. **58**, 1499 (1987).

[2] F. O. Farrbach, P. Simon, and A. Rohrbach, Microscopy with self-reconstructing beams, Nat. Photon. **4**, 780 (2010).

[3] V. Garces-Chavez, D. McGloin, H. Melville, W. Sibbett, and K. Dholakia, Simultaneous micromanipulation in multiple planes using a self-reconstructing light beam, Nature **419**, 145 (2002).

[4] G. A. Siviloglou, J. Broky, A. Dogariu, and D. N. Christodoulides, Observation of accelerating Airy beams, Phys. Rev. Lett. **99**, 213901 (2007).

[5] J. Broky, G. A. Siviloglou, A. Dogariu, and D. N. Christodoulides, Self-healing properties of optical Airy beams, Opt. Express **16**, 12880 (2008).

[6] J. Baumgartl, M. Mzzilu, and K. Dholakia, Optically mediated particle clearing using Airy wavepackets, Nat. Photon. **2**, 675 (2008).

[7] P. Polynkin, M. Kolesik, J. V. Moloney, G. A. Siviloglou, and D. N. Christodoulides, Curved plasma channel generation using ultraintense Airy beams, Science **324**, 229 (2009).

[8] R. Dorn, S. Quabis, and G. Leuchs, Sharper focus for a radially polarized light beam, Phys. Rev. Lett. **91**, 233901 (2003).

[9] P. Wróbel, J. Pniewski, T. J. Antosiewicz, and T. Szoplik, Focusing radially polarized light by a concentrically corrugated silver film without a hole, Phys. Rev. Lett. **102**, 183902 (2009).

[10] L. Novotny, M. R. Beversluis, K. S. Youngworth, and T. G. Brown, Longitudinal field modes probed by single molecules, Phys. Rev. Lett. **86**, 5251 (2001).

[11] Q. Zhan, Cylindrical vector beams: From mathematical concepts to applications, Adv. Opt. Photon. **1**, 1 (2009).

[12] K. S. Youngworth and T. G. Brown, Focusing of high numerical aperture cylindrical-vector beams, Opt. Express **7**, 77 (2000).

[13] L. Allen, M. W. Beijersbergen, R. J. C. Spreeuw, and J. P. Woerdman, Orbital angular momentum of light and the transformation of Laguerre-Gaussian laser modes, Phys. Rev. A **45**, 8185 (1992).

[14] J. Wang, J. Yang, I. Fazal, N. Ahmed, Y. Yan, H. Huang, Y. Ren, Y. Yue, S. Dolinar, M. Tur, and A. Willner, Terabit free-space data transmission employing orbital angular momentum multiplexing, Nat. Photon. **6**, 488 (2012).

[15] G. Molina-Terriza, J. P. Torres, and L. Torner, Twisted photons, Nat. Phys. **3**, 305 (2007).

[16] K. Dholakia and T. Cizmar, Shaping the future of manipulation, Nat. Photon. **5**, 335 (2011).

[17] Y. Kato, K. Mima, N. Miyanaga, S. Arinaga, Y. Kitagawa, M. Nakatsuka, and C. Yamanaka, Random phasing of high-power lasers for uniform target acceleration and plasma-instability suppression, Phys. Rev. Lett. **53**, 1057 (1984).

[18] Y. Cai and S. Zhu, Ghost imaging with incoherent and partially coherent light radiation, Phys. Rev. E **71**, 056607 (2005).

[19] T. E. Gureyev, D. M. Paganin, A. W. Stevenson, S. C. Mayo, and S. W. Wilkins, Generalized eikonal of partially coherent beams and its use in quantitative imaging, Phys. Rev. Lett. **93**, 068103 (2004).

[20] J. N. Clark, X. Huang, R. Harder, and I. K. Robinson, High-resolution three-dimensional partially coherent diffraction imaging, Nat. Commun. **3**, 993 (2012).

[21] J. Zhang, Z. Wang, B. Cheng, Q. Wang, B. Wu, X. Shen, L. Zheng, Y. Xu, and Q. Lin, Atom cooling by partially spatially coherent lasers, Phys. Rev. A **88**, 023416 (2013).

[22] G. R. M. Robb and W. J. Firth, Collective atomic recoil lasing with a partially coherent pump, Phys. Rev. Lett. **99**, 253601 (2007).

[23] J. C. Ricklin and F. M. Davidson, Atmospheric turbulence effects on a partially coherent Gaussian beam: Implications for free-space laser communication, J. Opt. Soc. Am. A **19**, 1794 (2002).

[24] C. Zhao and Y. Cai, Trapping two types of particles using a focused partially coherent elegant Laguerre–Gaussian beam, Opt. Lett. **36**, 2251 (2011).

[25] Y. Dong, F. Wang, C. Zhao, and Y. Cai, Effect of spatial coherence on propagation, tight focusing, and radiation forces of an azimuthally polarized beam, Phys. Rev. A **86**, 013840 (2012).

[26] T. vanDijk, D. G. Fischer, T. D. Visser, and E. Wolf, Effects of spatial coherence on the angular distribution of radiant intensity generated by scattering on a sphere, Phys. Rev. Lett. **104**, 173902 (2010).

[27] C. Ding, Y. Cai, O. Korotkova, Y. Zhang, and L. Pan, Scattering-induced changes in the temporal coherence length and the pulse duration of a partially coherent plane-wave pulse, Opt. Lett. **36**, 517 (2011).

[28] M. S. Zubairy and J. K. McIver, Second-harmonic generation by a partially coherent beam, Phys. Rev. A **36**, 202 (1987).

[29] Y. Cai and U. Peschel, Second-harmonic generation by an astigmatic partially coherent beam, Opt. Express **15**, 15480 (2007).

[30] E. Wolf, *Introduction to the Theory of Coherence and Polarization of Light* (Cambridge University Press, Cambridge, 2007).

[31] O. Korotkova and E. Wolf, Changes in the state of polarization of a random electromagnetic beam on propagation, Opt. Commun. **246**, 35 (2005).

[32] E. Wolf, Non-cosmological redshifts of spectral lines, Nature **326**, 363 (1987).

[33] E. Wolf, Red shifts and blue shifts of spectral lines emitted by two correlated sources, Phys. Rev. Lett. **58**, 2646 (1987).

[34] R. Simon, E. C. G. Sudarshan, and N. Mukunda, Anisotropic Gaussian Schell-model beams: Passage through optical systems and associated invariants, Phys. Rev. A **31**, 2419 (1985).

[35] Y. Cai and S. Zhu, Orbital angular moment of a partially coherent beam propagating through an astigmatic ABCD optical system with loss or gain, Opt. Lett. **39**, 1968 (2014).

[36] L. Mandel and E. Wolf, *Optical Coherence and Quantum Optics* (Cambridge University Press, Cambridge, 1995).

[37] Y. Cai, Generation of various partially coherent beams and their propagation properties in turbulent atmosphere: A review, Proc. SPIE **7924**, 792402 (2011).

[38] Y. Cai, F. Wang, C. Zhao, S. Zhu, G. Wu, and Y. Dong, in *Vectorial Optical Fields: Fundamentals and Applications*, edited by Q. Zhen (World Scientific, Singapore, 2013), Chap. 7, pp. 221–273.

[39] F. Gori and M. Santarsiero, Devising genuine spatial correlation functions, Opt. Lett. **32**, 3531 (2007).

[40] F. Gori, V. R. Sanchez, M. Santarsiero, and T. Shirai, On genuine cross-spectral density matrices, J. Opt. A: Pure Appl. Opt. **11**, 085706 (2009).

[41] Y. Cai, Y. Chen, and F. Wang, Generation and propagation of partially coherent beams with nonconventional correlation functions: a review [Invited], J. Opt. Soc. Am. A **31**, 2083 (2014).

[42] H. Lajunen and T. Saastamoinen, Propagation characteristics of partially coherent beams with spatially varying correlations, Opt. Lett. **36**, 4104 (2011).

[43] S. Sahin and O. Korotkova, Light sources generating far fields with tunable flat profiles, Opt. Lett. **37**, 2970 (2012).

[44] F. Wang, C. Liang, Y. Yuan, and Y. Cai, Generalized multi-Gaussian correlated Schell-model beam: from theory to experiment, Opt. Express **22**, 23456 (2014).

[45] Z. Mei and O. Korotkova, Random sources generating ring-shaped beams, Opt. Lett. **38**, 91 (2013).

[46] F. Wang, X. Liu, Y. Yuan, and Y. Cai, Experimental generation of partially coherent beams with different complex degrees of coherence, Opt. Lett. **38**, 1814 (2013).

[47] C. Liang, F. Wang, X. Liu, Y. Cai, and O. Korotkova, Experimental generation of cosine-Gaussian-correlated Schell-model beams with rectangular symmetry, Opt. Lett. **39**, 769 (2014).

[48] Y. Yuan, X. Liu, F. Wang, Y. Chen, Y. Cai, J. Qu, and H. T. Eyyuboğlu, Scintillation index of a multi-Gaussian Schell-model beam in turbulent atmosphere, Opt. Commun. **305**, 57 (2013).

[49] Y. Gu and G. Gbur, Scintillation of nonuniformly correlated beams in atmospheric turbulence, Opt. Lett. **38**, 1395 (2013).

[50] Y. Chen, F. Wang, L. Liu, C. Zhao, Y. Cai, and O. Korotkova, Generation and propagation of a partially coherent vector beam with special correlation functions, Phys. Rev. A **89**, 013801 (2014).

[51] Y. Chen and Y. Cai, Generation of a controllable optical cage by focusing a Laguerre–Gaussian correlated Schell-model beam, Opt. Lett. **39**, 2549 (2014).

[52] J. Bucay, E. Roussel, J. O. Vasseur, P. A. Deymier, A. C. Hladky-Hennion, Y. Pennec, K. Muralidharan, B. Djafari-Rouhani, and B. Dubus, Positive, negative, zero refraction, and beam splitting in a solid/air phononic crystal: Theoretical and experimental study, Phys. Rev. B **79**, 214305 (2009).

[53] J. Zhao, Y. Chen, and Y. Feng, Polarization beam splitting through an anisotropic metamaterial slab realized by a layered metal-dielectric structure, Appl. Phys. Lett. **92**, 071114 (2008).

[54] P. Halevi, Beam splitting by a plane-parallel absorptive slab, Opt. Lett. **7**, 469 (1982).

[55] Z. Sun, Beam splitting with a modified metallic nano-optic lens, Appl. Phys. Lett. **89**, 261119 (2006).

[56] L. A. Romero and F. M. Dickey, Theory of optimal beam splitting by phase gratings. I. One-dimensional gratings, J. Opt. Soc. Am. A **24**, 2280 (2007).

[57] Y. Cai and S. Zhu, Ghost interference with partially coherent radiation, Opt. Lett. **29**, 2716 (2004).

[58] A. Ashkin, J. M. Dziedzic, J. E. Bjorkholm, and S. Chu, Observation of a single-beam gradient force optical trap for dielectric particles, Opt. Lett. **11**, 288 (1986).

[59] D. Cassettari, B. Hessmo, R. Folman, T. Maier, and J. Schmiedmayer, Beam splitter for guided atoms, Phys. Rev. Lett. **85**, 5483 (2000).

[60] A. E. Siegman, New developments in laser resonators, Proc. SPIE **1224**, 2 (1990).

[61] F. Gori, M. Santarsiero, and A. Sona, The change of width for a partially coherent beam on paraxial propagation, Opt. Commun. **82**, 197 (1991).

[62] M. Santarsiero, F. Gori, R. Borghi, G. Cincotti, and P. Vahimaa, Spreading properties of beams radiated by partially coherent Schell-model sources, J. Opt. Soc. Am. A **16**, 106 (1999).

[63] S. A. Collins, Lens-system diffraction integral written in terms of matrix optics, J. Opt. Soc. Am. **60**, 1168 (1970).

[64] Q. Lin and Y. Cai, Tensor ABCD law for partially coherent twisted anisotropic Gaussian-Schell model beams, Opt. Lett. **27**, 216 (2002).

[65] P. de. Santis, F. Gori, G. Guattari, and C. Palma, An example of a Collett-Wolf source, Opt. Commun. **29**, 256 (1979).